

Mechanical and Shape-Memory Properties of Polyamide/Maleated Polyethylene/Linear Low-Density Polyethylene Blend

Guo-Ming Lin, Guo-Xin Sui, Rui Yang

Institute of Metal Research, Chinese Academy of Sciences, Shenyang 110016, People's Republic of China

Received 21 October 2011; accepted 28 January 2012

DOI 10.1002/app.36911

Published online in Wiley Online Library (wileyonlinelibrary.com).

ABSTRACT: Novel polymer blends of polyamide and linear low-density polyethylene with maleated polyethylene as compatibilizers were prepared in a modular intermeshing corotating twin-screw extruder. Polymer blends with different contents of polyamide in polyethylene matrix were obtained. The mechanical properties were studied in terms of the tensile strength and elongation-to-break. The shape-memory properties of the blended materials were characterized using three-point bending test in a temperature-controlled chamber. The results show that

the incorporation of maleated polyethylene has a strong effect on the tensile properties and the morphology of the blends. The shape-memory effect of blended materials is affected by polyamide weight fraction, and 60 wt % polyethylene, 20 wt % polyamide, and 20% maleated polyethylene have an acceptable performance. © 2012 Wiley Periodicals, Inc. *J Appl Polym Sci* 000: 000–000, 2012

Key words: polymer blend; mechanical properties; shape-memory polymer

INTRODUCTION

Shape-memory materials are one type of smart materials which can return to their permanent shapes from memorizing temporary shapes under external stimuli such as temperature, moisture, pH, light, electric field, magnetic field, and specific ions or enzyme.¹ Over shape-memory metallic alloys and shape-memory ceramics, shape-memory polymers (SMPs) have many advantages including light weight, low cost, excellent processability, high shape deformability, high shape recoverability, and tailorable switch temperature. Among SMPs, thermoresponsive SMP is a typical one, which has been widely studied and used in industry. Li et al. reported several shape-memory graft copolymers with physical crosslinking.^{2–4} Chen et al. reported a two-way shape-memory polyurethane composites based on the changing of strength of elastic PU with temperature.⁵ Lendlein et al. explored a series of biodegradable, amorphous, shape-memory polyurethane networks by incorporation of different comonomers and discussed the controlling of switching temperature.⁶ Lendlein and Kelch reviewed the fundamental aspects of the molecular design of suitable polymer architectures, the programming and recover processes, and the quantification of the shape-memory

effect.⁷ Among various SMPs, polymer-blended SMPs have attracted great attentions owing to their controllability and their amenability to fabrication.

Theoretically, for a polymer to possess shape-memory capability, it should have a permanent network and a reversible phase.⁷ The permanent network is designed to memory the permanent shape and the fixing of temporary shapes, on the other hand, is owing to the reversible phase. The recent study on SMP is abundant. Generally, recent SMPs can be classified into two main categories. One is copolymers with covalently crosslinked or physically crosslinked.^{8–10} The other is polymer blends which are usually consisted of two polymers.^{9,11–13} One plays a role of the reversible phase and the other acts as the permanent network. Generally, these two polymers are required to be melt-miscible, and the melting point (T_m) of the former polymer is referred to as the switching temperature.

Polymer blending offers a simple way to fabricate SMPs. Block or graft copolymers formed by *in situ* reaction of the blend components with compatibilizer precursors have been extensively investigated for polyethylene (PE)/polyamide (PA) and other blends.^{14–24} Several articles about polyolefin-based blends are in the literature, using different compatibilizers, such as acrylic acid, phosphazene compounds,²⁵ ionomers,^{26,27} and maleic anhydride.^{22,28,29} In this article, a miscibility shape-memory blend was designed with the PA 6 and linear low-density polyethylene (LLDPE) as the two principal components. Maleated PE was added as compatibilizer. The

Correspondence to: G.-X. Sui (gxsui@imr.ac.cn).

miscibility between PA and PE and the presence of compatibilizer form the shape-memory molecular design theoretically. The miscibility, thermal and mechanical properties, and the relationship between phase morphology and shape-memory properties were studied in this article. Finally, a mechanism and an optimization design for this type of SMP blend were proposed and testified.

EXPERIMENTAL

Materials

LLDPE (KunLun, Petrochina Daqing Petrochemical, China, density of 0.92 g/cm³, melting point of 122.2°C, melt flow index [MFI], 1.9 g/10 min) and PA 6 (Jisheng Corporation in Taipei, China, density of 1.12 g/cm³, melting point of 222.4°C, MFI, 2.5 g/10 min) were used as blend components. The maleated PE (PE-G, Nanjing Debasuhua in Nanjing, China, density of 0.93 g/cm³, melting point of 113.1°C, MFI, 2.0 g/10 min) were added as compatibilizers.

Specimen preparation

The compounding of SMP blend was achieved by using twin-screw extruder with a screw speed of 360 rpm under processing temperature of 220°C. All the materials were dried in a vacuum chamber at 80°C for 24 h prior to melt processing. The extrudate was continuously cooled by water and pelletized. The pellets were dried in oven at 80°C for 24 h, ready for injection molding. Standard test bars were injection molded with material temperature at 230°C and mold temperature at 80°C.

Thermal analysis

Differential scanning calorimetry (DSC) analysis was taken on a TA DSC Q20 instrument (USA) protected by nitrogen atmosphere. After being dried in a vacuum at 80°C for 24 h, about 8 mg of samples was weighed accurately in an aluminum pan and melted at 250°C for 5 min to eliminate the thermal history. Then, they were cooled to 50°C and reheated to 250°C. Both heating and cooling rates were 5°C/min.

Morphological observation

The microstructures of the blends were observed by scanning electron microscope (SEM; JEOL JSM 6301F; Japan). All samples were cryogenically fractured by liquid nitrogen. Most of the blends were studied by preferential etching of the PA phase in formic acid for 24 h and the fractured surfaces were coated with a thin layer of gold prior to analysis.

Mechanical properties

Tensile tests were carried out on a universal testing machine with a crosshead speed of 20.0 mm/min,

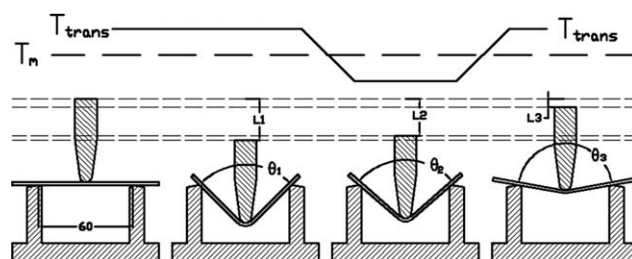


Figure 1 Three-point bending test of shape-memory experiments.

according to ASTM D638 M. A load cell of 2 kN and an extensometer with a gauge length of 25 mm were used. The parallel segment of the dumbbell-shaped specimens for tensile tests was in a size of 57 × 10 × 3.5 mm. For each specimen, the data reported here represented the averaged result of at least five successful tests.

Characterization of shape-memory properties

A three-point bending test in a temperature-controlled chamber was employed to evaluate the shape-recovery properties. The size of the flat strip specimen was 100 × 25 × 2 mm. The test apparatus is shown in Figure 1. The specimen was first deformed to θ_1 at a deformation temperature (T_{trans}) about 125°C, which was higher than T_m of the PE, by the L_1 movement of the crosshead. While maintaining the crosshead, the specimen was cooled to -40°C for 10 min to fix the temporary shape. After freeing the cross head, a small recovery occurred and the specimen deformation changed to θ_2 . This bended specimen was subsequently heated to T_{trans} again, and its recovery behavior occurred. The deformation angle of the specimen was θ_3 , and the position of the cross head was L_3 . Shape-fixing ratio, R_f , and shape-recovery ratio, R_r , were defined by eqs. (1) and (2), and were calculated by eqs. (3) and (4) in which the L_1 , L_2 , and L_3 were defined in Figure 1 instead of θ_1 , θ_2 , and θ_3 which could not be measured easily.⁷

$$R_f = \frac{\pi - \theta_2}{\pi - \theta_1} \times 100\% \quad (1)$$

$$R_r = \left(\frac{(\pi - \theta_1) - (\pi - \theta_3)}{\pi - \theta_1} \right) \times 100\% \quad (2)$$

$$R_f = \frac{\pi - 2\text{arccot} \frac{L_2}{30}}{\pi - 2\text{arccot} \frac{L_1}{30}} \times 100\% \quad (3)$$

$$R_r = \frac{2\text{arccot} \frac{L_3}{30} - 2\text{arccot} \frac{L_1}{30}}{\pi - 2\text{arccot} \frac{L_1}{30}} \times 100\% \quad (4)$$

RESULTS AND DISCUSSION

Microstructures of PA/LLDPE/PE-G blends

The SEM micrographs of original freeze-fractured surfaces of blends with 20% PA and different

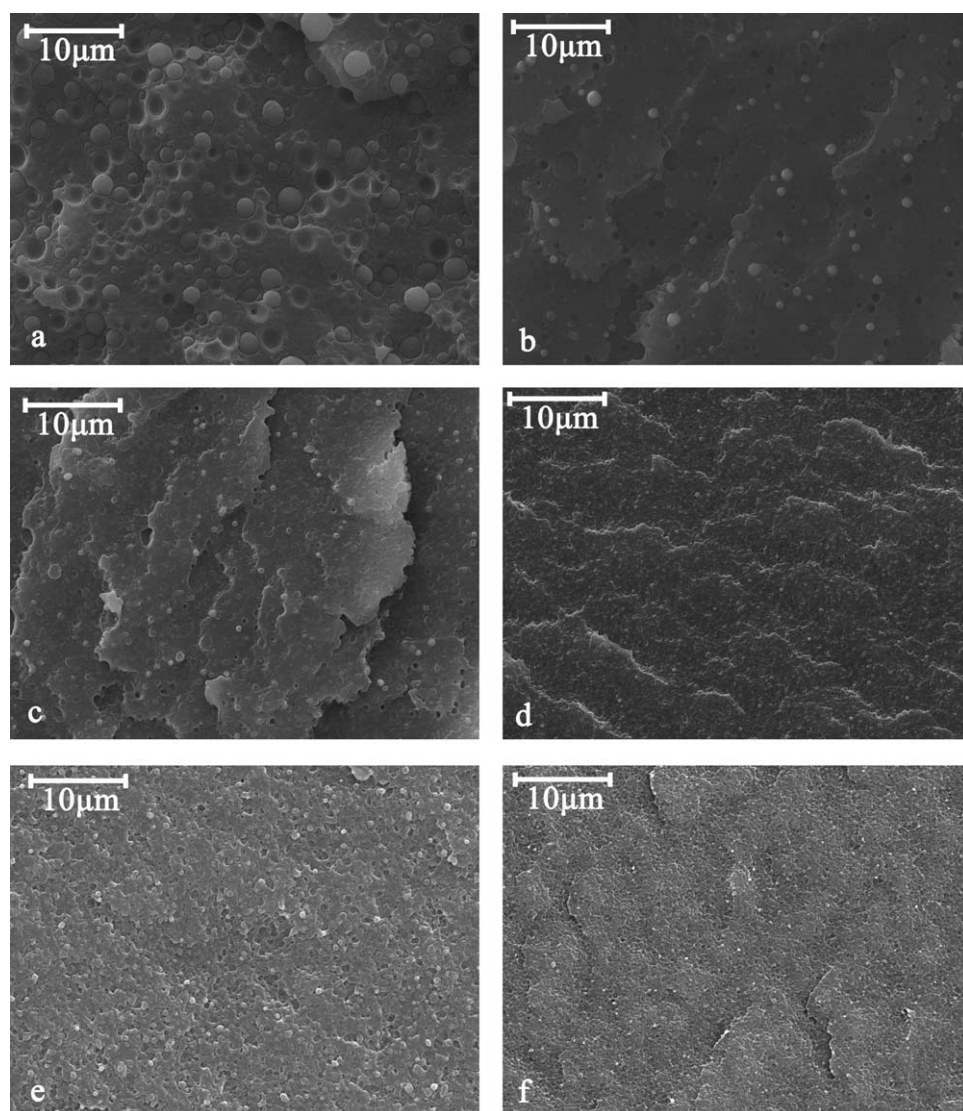


Figure 2 The SEM micrographs of the original typical PA/LLDPE/PE-G blend samples with 20% PA. (a) 0% PE-G, (b) 10%PE-G, (c) 15% PE-G, (d) 20% PE-G, (e) 30% PE-G, and (f) 40% PE-G.

contents of PE-G are shown in Figure 2. To observe the microstructure of blends clearly, the PA domains are preferentially etched by dipping the samples in formic acid for 24 h. The SEM micrographs of those PA domains are shown in Figure 3 in which the black domains indicate the position of the extracted PA phase. It is clearly seen that PA phase is dispersed in the LLDPE matrix as spherical domains without PE-G as shown in Figure 2(a). Obviously, the compatibility between the LLDPE matrix and the PA-phase domains is poor.³⁰ As expected, large particles of several micrometers (the radius of 80% particles are larger than 1micrometer) appear in blends without PE-G, dispersed phase with large domain size shown in Figure 3(a) indicates poor interfacial adhesion. The shape of PA dispersed phase is spherical and the average size of PA is about 2.6 μm . On the other hand, it is shown that PE-G enhances

the adhesion of PA domains to the LLDPE matrix [Fig. 2(b–d)]. The individual PA domains are visible at the surface, whereas the size of PA domains became smaller with increasing PE-G. When PE-G was added as compatibilizer, a decrease in the size of PA-phase domain is observed [Fig. 3(b–d)]. Meanwhile, the PA-phase domain is elongated. There is good interfacial adhesion between the phases.³¹ There are few differences in Figure 3(d–f), which indicate that 20% PE-G is enough for the blends with 20% PA.

The content of PA has an obvious effect on the microstructure of blend. The transformation is shown in Figure 4. All samples are dipped in formic acid for 24 h. When the content is 5%, PA phase is in a droplet-like dispersion. With the increasing of PA, more black domains of PA phase show up in the micrographs. The size of PA phases changes a

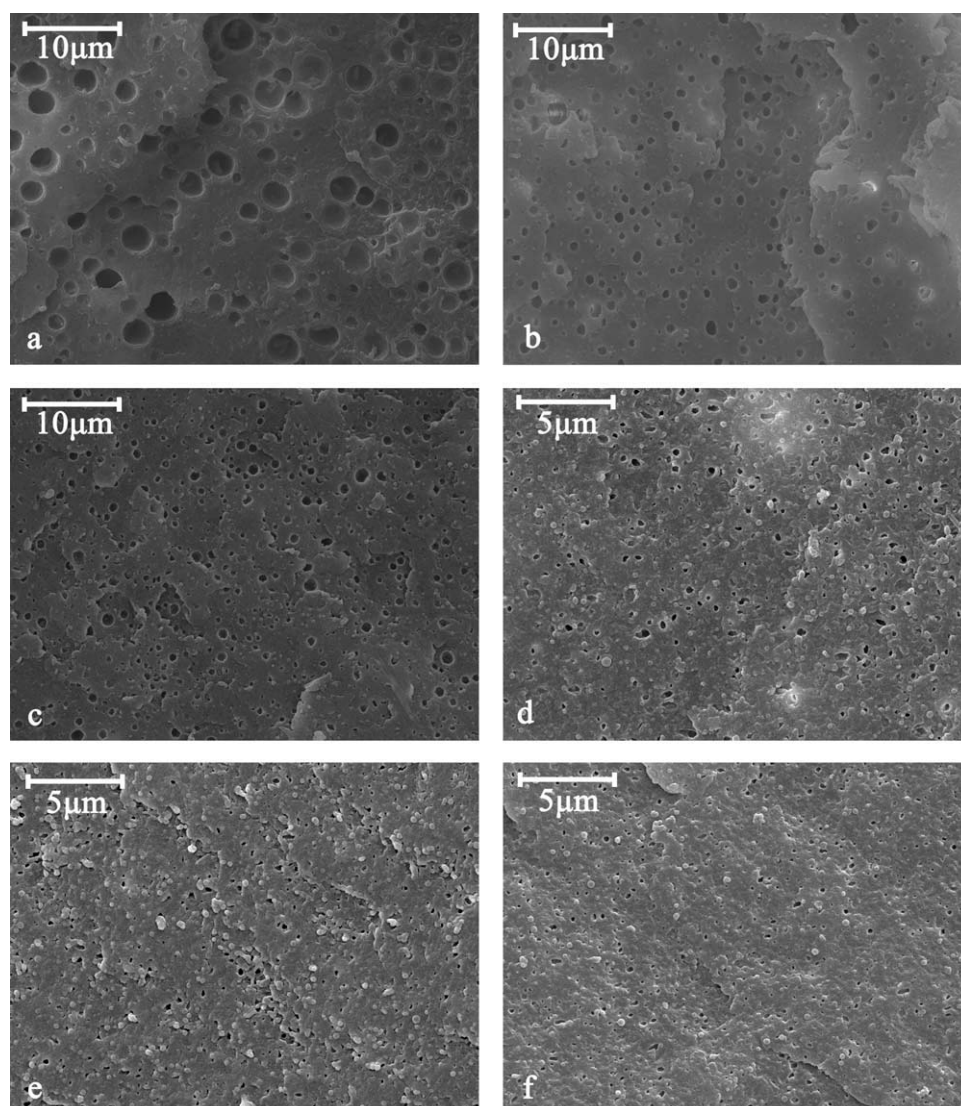


Figure 3 The SEM micrographs of etched PA/LLDPE/PE-G blend samples with 20% PA (black holes are etched PA domains and others including particles are matrix). (a) 0% PE-G, (b) 5% PE-G, (c) 10% PE-G, (d) 20% PE-G, (e) 30% PE-G, and (f) 40% PE-G.

little until the PA content reaches 30%. When the content of PA reaches 30%, the size of the PA phases grows up suddenly and the maximum size of PA phase is about 1.8 μm .

It is clear from the above discussion that the samples with approximate 20% PE-G have acceptable PA morphology. They were obtained under our preparation condition as described in Specimen preparation section. These phase morphology analyses are helpful to understand the mechanical properties and shape-memory properties of the PA/LLDPE blends.

Miscibility of PA/LLDPE/PE-G blend

The thermal properties of PA/LLDPE/PE-G blends were determined by DSC. The DSC plots of each sample labeled from PE-G0 to PE-G50 are shown in

Figure 5(a). The DSC plots of each sample labeled from PA0 to PA40 are shown in Figure 5(b). The details of Figure 5(a,b) are shown in Tables I and II.

Melting points of the PA/LLDPE/PE-G blend systems with different compositions are listed in Table I for the discussion of the miscibility among three components. The T_m s of LLDPE and PA in sample PEG0 show no change and this indicates the immiscibility between the two components, which is consistent with the literature.¹⁸ For samples PE-G5, PE-G10, and PE-G20, the T_m s of LLDPE could be obviously determined. The T_m s of LLDPE shift from 122.2 to 126.7°C and become wider as summarized in Table I, which indicates that PE-G is a good compatibilizer between PA and LLDPE. For samples with more PE-G, the T_m s of LLDPE and PA cannot approach further to each other but fluctuate around 125.5 and 221°C, respectively. When the content of

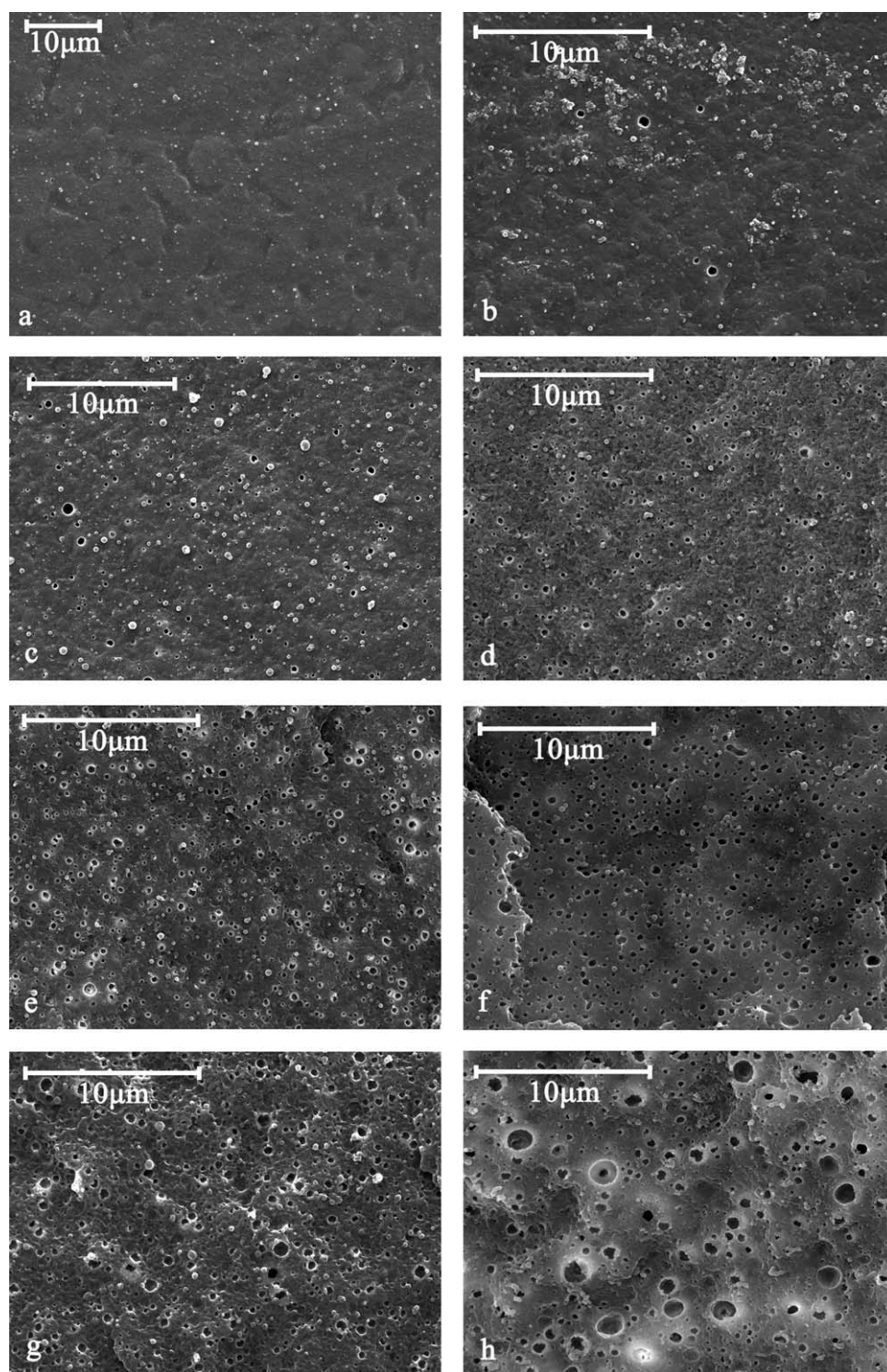


Figure 4 The SEM micrographs of typical PA/LLDPE/PE-G blend samples with 20% PE-G (black holes are etched PA domains and others including particles are matrix). (a) 0% PA, (b) 5% PA, (c) 10% PA, (d) 15% PA, (e) 20% PA, (f) 25% PA, (g) 30% PA, and (h) 35% PA.

PE-G is more than 25%, the compatibilizer is enough and the thermal properties of blends are stable. When the PE-G content is fixed at 20%, the T_m s of LLDPE fluctuate around 124.5°C with different PA6 loadings as listed in Table II, which indicates that the T_m s of LLDPE are impacted only by PE-G.

It is clear from the above results that the immiscibility between LLDPE and PA could be confirmed and PE-G is a good compatibilizer for the system. Thus, the relationship among the three components could induce the morphology of phase separation in blends.

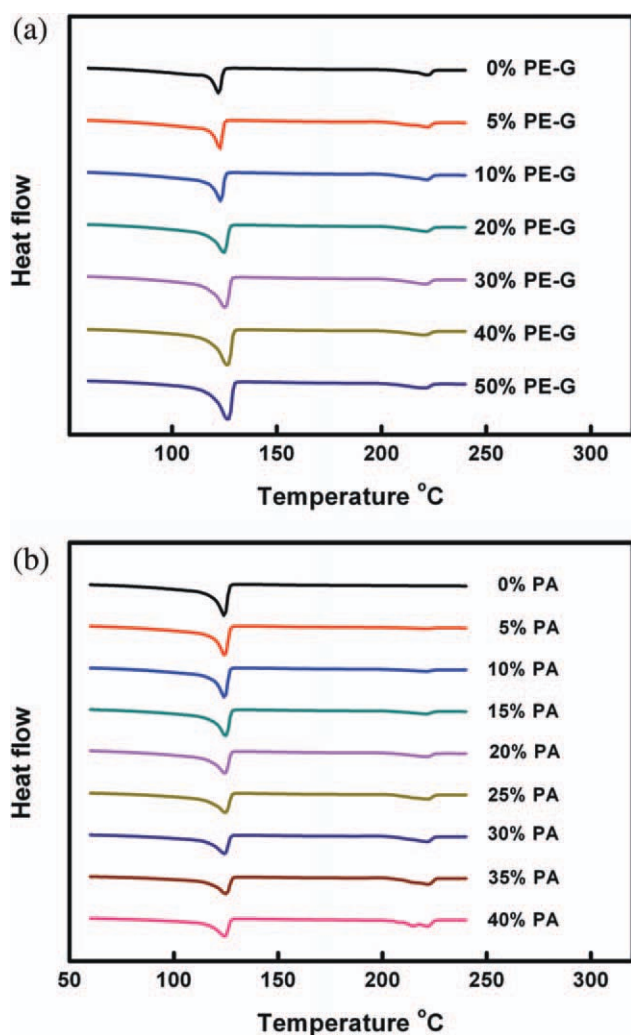


Figure 5 The DSC plots of blends. (a) Different contents of PE-G with 20% PA and (b) different contents of PA with 20% PE-G, pure PE and PA. [Color figure can be viewed in the online issue, which is available at wileyonlinelibrary.com.]

Mechanical properties of PA/LLDPE/PE-G blends

The mechanical properties of blends were characterized by tensile tests at room temperature. The dependence of tensile strength, elongation at break, Young's modulus on PE-G and PA contents is shown in Figures 6 and 7.

TABLE I
The Details of Figure 5(a)

PEG (%)	T_m of PE (°C)	T_m of PA (°C)
0	122.2	222.4
5	123.8	222.3
10	124.7	221.9
20	125.2	221.5
30	125.5	221.4
40	125.41	220.8
50	125.7	221

As shown in Figure 6, the tensile strength and elongation at fracture show the trend as a function of the PE-G contents and Young's modulus fluctuate around 550 MPa with the increasing of PE-G. Two important features should be noted in Figure 6. The tensile strength of blends does not increase linearly with the increasing of PE-G. When the content of PE-G exceeds 20%, the tensile strength rises slowly. The elongation at fracture is reduced when the PE-G content is more than 30%. The Young's moduli of SMPs fluctuate around 550 MPa in Figure 6. The size of PA-phase domain cannot change the Young's modulus of blends.

The trend of the tensile strength, Young's modulus, and elongation at fracture as a function of the PA content is clearly shown in Figure 7. The tensile strength increases from 15.8 to 32.7 MPa, whereas the contents of PA increase from 0 to 40%. The Young's modulus mounts up from 332.8 to 981 MPa and elongation at fracture decreases from 551.7 to 237.4% at the same time. They follow the common knowledge.

Generally speaking, it is shown in Figures 6 and 7 that the 20% PE-G could play an important role as compatibilizer in the blends. During the tensile tests, no delamination of the samples was observed. In view of the immiscibility between PA and LLDPE, the adhesion between the two phases was supposed to be low. But from the SEM micrographs, the phase sizes were only in the range of several microns. The topology of the microphase separation morphology may be helpful to prevent the macro-scale delamination.

Shape-memory properties of PA/LLDPE/PE-G blend

The T_m s of LLDPE (120–130°C) could be taken as the shape-memory transition temperatures (T_{trans}) of the blends. The detailed shape-memory properties were represented by shape-recovery ratio (R_r) and shape-fixing ratio (R_f) according to Characterization of shape-memory properties section. R_r and R_f of the

TABLE II
The Details of Figure 5(b)

PA (%)	T_m of PE (°C)	T_m of PA (°C)
0	122.2	
5	123.5	220.2
10	124.3	220.5
15	124.8	220.9
20	124.5	221.1
25	124.6	221.2
30	124.4	222.0
35	125.0	222.1
40	124.5	222.0

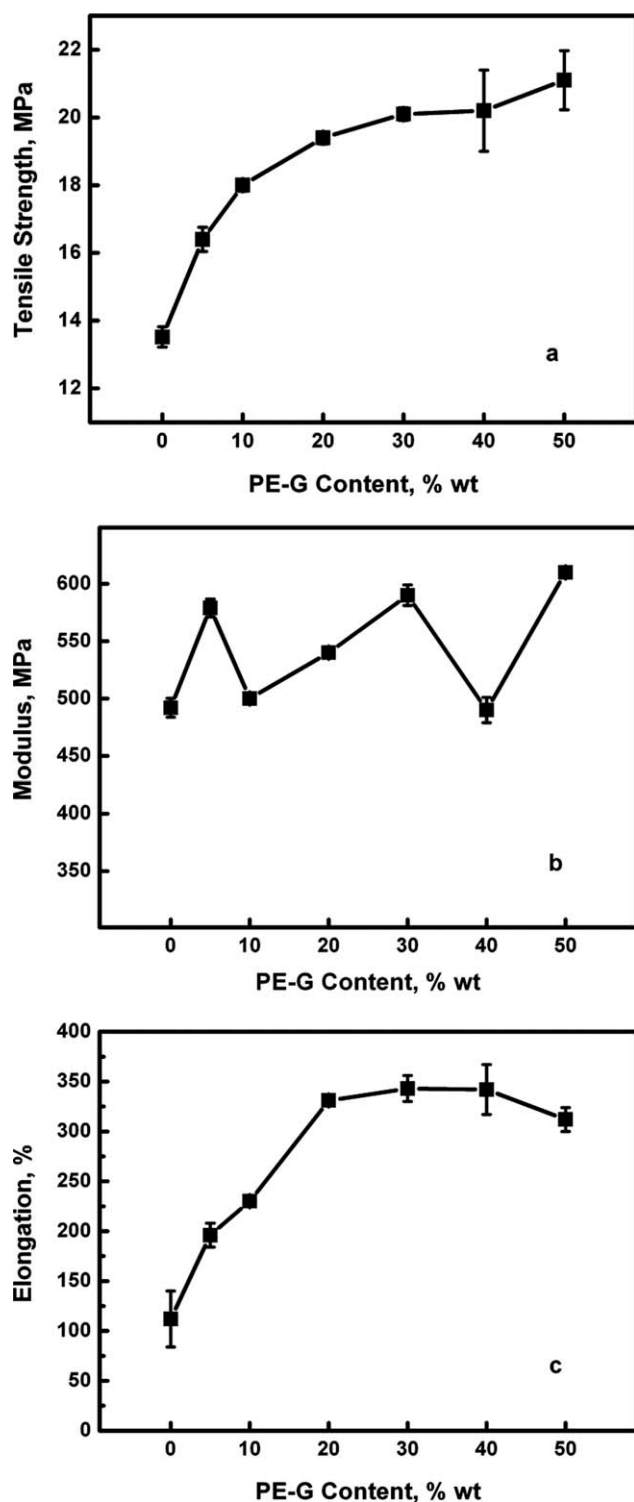


Figure 6 The mechanical properties of typical PA/LLDPE/PE-G blend samples with 20% PA.

PA/LLDPE/PE-G blend samples are calculated and shown in Figure 8 and the details are summarized in Table III. As shown in Figure 8, the R_r shifts from about 60 to 90% after the content of PA exceeds 15 wt % and R_f dropped from about 100 to 80% after PA content of 30 wt %. It is indicated that the micro-

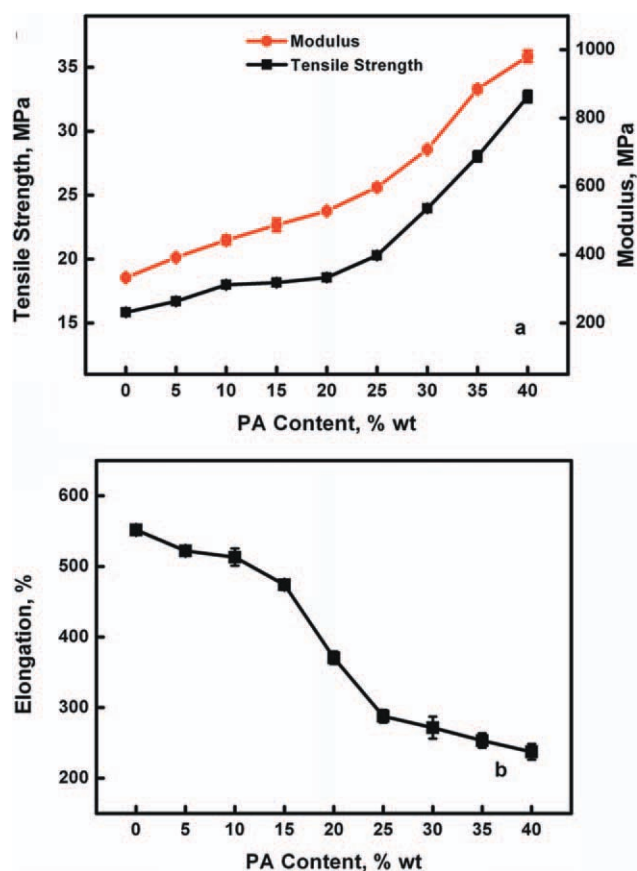


Figure 7 The mechanical properties of typical PA/LLDPE/PE-G blend samples with 20% PE-G. [Color figure can be viewed in the online issue, which is available at wileyonlinelibrary.com.]

structures of PA contributed to shape-recovery performance (R_r) and the melting of LLDPE contributed to shape-fixing performance (R_f). The curves shown in Figure 8 are divided into three regions for further discussion.

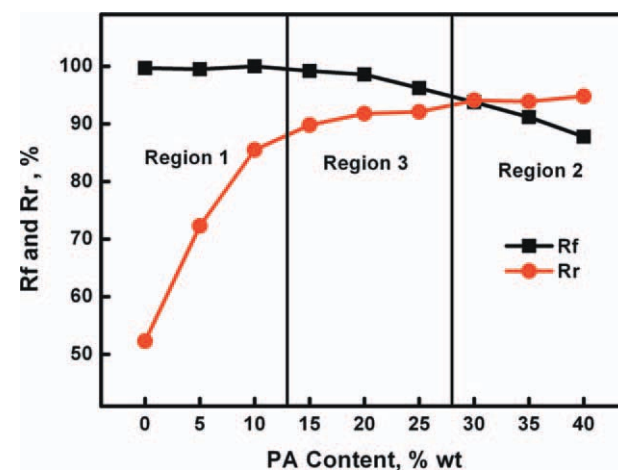


Figure 8 Shape-recovery ratio (R_r) and shape-fixing ratio (R_f) of each sample. [Color figure can be viewed in the online issue, which is available at wileyonlinelibrary.com.]

TABLE III
The Details of Figure 8

Contents	Shape fixing (%)	Shape recovery (%)
	R_f	R_r
80% LLDPE + 20% PE-G	99.7	52.3
5% PA + 75% LLDPE + 20% PE-G	99.5	72.3
10% PA + 70% LLDPE + 20% PE-G	100	85.5
15% PA + 65% LLDPE + 20% PE-G	99.2	89.8
20% PA + 60% LLDPE + 20% PE-G	98.6	91.8
25% PA + 55% LLDPE + 20% PE-G	96.2	92.1
30% PA + 50% LLDPE + 20% PE-G	93.8	94.1
35% PA + 45% LLDPE + 20% PE-G	91.2	93.9
40% PA + 40% LLDPE + 20% PE-G	87.8	94.8

Region 1 showed bad-shape recovery performance but good-shape fixing performance. The LLDPE matrix resulted in good-shape fixing performance and the little dispersed PA droplet phase [Fig. 4(a–c)] resulted in the low-grade of R_r . The distance between PA-phase domains is $>5 \mu\text{m}$ as shown in Figure 4(b). PA-phase domains could not form stable physical netpoints in the LLDPE matrix. The chain of LLDPE gets enough flexibility above the T_m and the permanent shape of shape-memory network is destroyed after the deformation process.

Region 2 showed good-shape recovery performance but deteriorated shape-fixing performance. The shape-recovery ratios (R_r) of these three samples are closed to 100%, which is owed to the multitudinous PA-phase domains [Fig. 4(g,h)]. For shape-fixing ratios (R_f), PA40 is much worse than PA20. The flexibility of LLDPE is limited because of the superabundant and big PA-phase domains in the LLDPE matrix shown in Figure 4(h).

Region 3 showed both good-shape recovery and good-shape fixing performances than PA5 and PA10. R_f and R_r of PA20 all exceed 90%, which was obtained from the improved microstructure of PA. When the contents of PA increase from 10 to 20%, more PA-phase domains exist [Fig. 4(c–e)]. These domains form stable physical netpoints. Therefore, the R_r increased to about 95%.

CONCLUSIONS

PA/LLDPE/PE-G blend is introduced as the example of a new type of polymer blend SMP system.

SEM and DSC results demonstrated the immiscibility between PA and LLDPE phases and PE-G plays an important role as compatibilizer. Shape-memory transition temperatures are in the range of 120–130°C. SEM micrographs and stress–strain curves clarified the phase-separation morphology.

According to the shape-memory investigation results, a shape-memory mechanism for this type of

polymer blend SMP proposed that the LLDPE of the blend contributed to shape-memory fixing performances and the PA of the blend under the help of PE-G contributed to shape-memory recovery performances. The PA provided the stretching and recovery performances and the LLDPE provided the fixing and unfixing performances.

The polymer blend with 60 wt % PE, 20 wt % PA, and 20% maleated PE have an acceptable performance. It is concluded that an optimized phase morphology can be designed to contain the LLDPE major continuous phase and PA dispersion phase.

References

- Meng, Q.; Hu, J. *Composites A: Appl Sci Manuf* 2009, 40, 1661.
- Li, F.; Chen, Y.; Zhu, W.; Zhang, X.; Xu, M. *Polymer* 1998, 39, 6929.
- Li, F.; Perrenoud, A.; Larock, R. C. *Polymer* 2001, 42, 10133.
- Andjelkovic, D. D.; Valverde, M.; Henna, P.; Li, F.; Larock, R. C. *Polymer* 2005, 46, 9674.
- Chen, S.; Hu, J.; Zhuo, H. *Composites Sci Technol* 2010, 70, 1437.
- Lendlein, A.; Zotzmann, J.; Feng, Y.; Altheld, A.; Kelch, S. *Biomacromolecules* 2009, 10, 975.
- Lendlein, A.; Kelch, S. *Angew Chem Int Ed* 2002, 41, 2035.
- Inomata, K.; Nakagawa, K.; Fukuda, C.; Nakada, Y.; Sugimoto, H.; Nakanishi, E. *Polymer* 2010, 51, 793.
- Kolesov, I. S.; Kratz, K.; Lendlein, A.; Radusch, H.-J. *Polymer* 2009, 50, 5490.
- Xie, T.; Rousseau, I. A. *Polymer* 2009, 50, 1852.
- Wang, L.-S.; Chen, H.-C.; Xiong, Z.-C.; Pang, X.-B.; Xiong, C.-D. *Mater Lett* 2010, 64, 284.
- Li, S.-C.; Lu, L.-N.; Zeng, W. *J Appl Polym Sci* 2009, 112, 3341.
- Zhang, H.; Wang, H.; Zhong, W.; Du, Q. *Polymer* 2009, 50, 1596.
- Pu, G.; Luo, Y.; Lou, Q.; Li, B. *Macromol Rapid Commun* 2009, 30, 133.
- Wang, D.; Li, Y.; Xie, X.-M.; Guo, B.-H. *Polymer* 2011, 52, 191.
- Shi, H. C.; Shi, D. A.; Wang, X. Y.; Yin, L. G.; Yin, J. H.; Mai, Y. W. *Polymer* 2010, 51, 4958.
- Padwa, A. R. *Polym Eng Sci* 1992, 32, 1703.
- Palabiyik, M.; Bahadur, S. *Wear* 2000, 246, 149.
- Dintcheva, N. T.; Filippone, G.; La Mantia, F. P.; Acierio, D. *Polym Degrad Stab* 2010, 95, 527.
- Therias, S.; Tzankova Dintcheva, N.; Gardette, J.-L.; La Mantia, F. P. *Polym Degrad Stab* 2010, 95, 522.
- Dayma, N.; Satapathy, B. K. *Mater Des* 2012, 33, 510.
- Jiang, C. H.; Filippi, S.; Magagnini, P. *Polymer* 2003, 44, 2411.
- Vallim, M. R.; Araujo, J. R.; Spinace, M. A. S.; De Paoli, M. A. *Polym Eng Sci* 2009, 49, 2005.
- Kudva, R. A.; Keskkula, H.; Paul, D. R. *Polymer* 1999, 40, 6003.
- Scaffaro, R.; Mistretta, M. C.; La Mantia, F. P.; Gleria, M.; Bertani, R.; Samperi, F.; Puglisi, C. *Macromol Chem Phys* 2006, 207, 1986.
- González-Núñez, R.; De Kee, D.; Favis, B. D. *Polymer* 1996, 37, 4689.
- Gonzalez-Núñez, R.; DeKee, D.; Favis, B. D. *Polymer* 1996, 37, 4689.
- Li, J.; Yu, X.; Guo, S. *J Polym Sci B: Polym Phys* 2007, 45, 184.
- Pan, L. H.; Inoue, T.; Hayami, H.; Nishikawa, S. *Polymer* 2002, 43, 337.
- Halldén, Å.; Deriss, M. J.; Wesslén, B. *Polymer* 2001, 42, 8743.
- Jiang, C.; Filippi, S.; Magagnini, P. *Polymer* 2003, 44, 2411.